

# Low-Energy Thermal Photons from Hadronic Matter

W. Liu and R. Rapp<sup>1</sup>

<sup>1</sup>*Cyclotron Institute and Physics Department, Texas A&M University, College Station, Texas 77843-3366*

(Dated: March 7, 2019)

Within an effective hadronic model including electromagnetic interactions via a  $U_{\text{em}}(1)$  gauge, we reinvestigate photon Bremsstrahlung from a hot hadronic gas as expected to be formed in relativistic heavy-ion collisions at SPS energies. We calculate photon emission from reactions of type  $\pi\pi \rightarrow \pi\pi\gamma$  and  $\pi K \rightarrow \pi K\gamma$  by an explicit (numerical) evaluation of the multi-dimensional phase space integral. This, in particular, allows to avoid the commonly employed soft photon approximation (SPA), as well as to incorporate final-state thermal enhancement factors. Both improvements are shown to result in an appreciable increase of the pertinent photon production over previous calculations. Upon convolution over a thermal fireball we find significant improvement in the description of recent WA98 data at low transverse momentum at SPS. The influence of both Landau-Pomeranchuk-Migdal and in-medium effects on “ $\sigma$ ” and  $\rho$ -meson exchanges are also discussed.

PACS numbers: relativistic heavy-ion collisions, photon spectra, Bremsstrahlung

## I. INTRODUCTION

A hot deconfined state of matter called quark-gluon plasma (QGP) is predicted to have existed during the first few microseconds after the big bang. Ultrarelativistic heavy-ion collisions (URHICs) provide the only way to recreate such matter for a short moment in the laboratory. Electromagnetic radiation is expected to be a unique probe in the study of URHICs, as the (real and virtual) photons, once produced, decouple from the strongly interacting hot matter. Since photons are emitted throughout the entire evolution of the fireball, including QGP and hadronic phases, their spectra carry valuable information on the various environments of their creation.

Studies of photon emission from hot and dense matter in heavy-ion collisions have a long history both theoretically and experimentally, cf., e.g., Refs. [1, 2, 3] for recent reviews. While scattering in deconfined matter is expected to predominantly manifest itself in the photon spectra at transverse-momenta above  $q_t \simeq 1.5$  GeV, the hadronic stages are likely to prevail the emission at low transverse momentum [4, 5, 6, 7, 8, 9, 10]. The latter regime has recently received renewed interest due to measurements of the WA98 collaboration in central  $Pb$ - $Pb$  collisions at the CERN Super Proton Synchrotron (SPS) [11, 12]. Using Hanbury Brown-Twiss (HBT) interferometry methods, a direct photon signal could be extracted in the transverse-momentum range of  $q_t = 0.1 - 0.3$  GeV [12]. These data exhibit large excess over theoretical predictions [9, 10] that have previously shown agreement with data for the same system (and by the same experiment) [11] at higher momenta,  $q_t \geq 1.5$  GeV (where the more conventional subtraction method enabled the extraction of a direct photon excess). In subsequent work [10, 13, 14], the role of photon Bremsstrahlung from elastic  $\pi$ - $\pi$  interactions, which was not included in the previous calculations, has been re-assessed. It was found that the Bremsstrahlung contribution notably increases the spectral yield at low  $q_t$  by up to 50% over the baseline predictions, but still significantly falls short of the WA98 data [12].

The main objective of the present work is to revisit thermal Bremsstrahlung from elastic meson-meson interactions. Based on an effective hadronic Lagrangian, with electromagnetic interactions implemented via  $U_{\text{em}}(1)$  gauging, we improve the accuracy of earlier analyses by going beyond the commonly employed soft photon approximation (SPA) [15], and extend the calculations to the strangeness sector ( $\pi$ - $K$  scattering). In the context of soft dileptons, corrections to the SPA have been found to be sizable and positive [16]. We furthermore complement our rate calculations by estimates of the Landau-Pomeranchuk-Migdal effect [17, 18], as well as a schematic treatment of medium effects on the scalar  $\pi$ - $\pi$  channel. Our approach enables, in particular, the explicit inclusion of thermal final-state enhancement factors, as well as meson-chemical potentials which arise in the hadronic evolution of URHICs after hadrochemical freezeout. The Bremsstrahlung rates are combined with earlier hadronic rate calculations [9] and convoluted over a thermal fireball model for central  $Pb$ - $Pb$  collisions at SPS in order to compare to the recent low-momentum WA98 data [12].

Our article is organized as follows. In Sec. II we introduce the chiral effective Lagrangian that will be used to evaluate amplitudes for elastic  $\pi$ - $\pi$  and  $\pi$ - $K$  interactions, with parameters fixed to reproduce the corresponding vacuum scattering data in Born approximation. In Sec. III, we discuss our treatment of the basic kinetic theory expression to calculate Bremsstrahlung from pion-pion and pion-kaon scattering in a thermal bath. We first construct in Sec. III A the pertinent scattering amplitudes by gauging the hadronic Lagrangian, with special care to maintain electromagnetic gauge invariance by implementing appropriate contact interactions (4-point vertices). We then give a detailed account of the various features that govern the emission rate in Sec. III B, with emphasis on the improvements over previous

evaluations. In Secs. IV and V, the influence of Landau-Pomeranchuk-Migdal (LPM) effect and (schematic) medium modifications of the meson-exchanges are explored, respectively. In Sec. VI, the soft photon production rate is applied to calculate photon spectra in central  $Pb$ - $Pb$  collisions at SPS, which are supplemented with earlier calculations and compared to experimental data from WA98. In Sec. VII, we estimate the coherent photon emission from initial scattering of protons within both projectile and target nuclei. A summary and discussion are contained in Sec. VIII.

## II. ELASTIC MESON-MESON SCATTERING

In this work we focus on photon Bremsstrahlung induced by elastic interactions of the lightest constituents in a hadronic gas, i.e., pion-pion ( $\pi$ - $\pi$ ) and pion-kaon ( $\pi$ - $K$ ) scattering (the latter will turn out to produce a factor of 4-5 less low-energy photons than the former; thus, contributions from  $K$ - $K$  scattering will be neglected). We first briefly describe the underlying model that will allow us reproduce vacuum scattering data and thus form the basis to evaluate the pertinent Bremsstrahlung processes,  $\pi^a \pi^b \rightarrow \pi^1 \pi^2 \gamma$  and  $\pi^a K^b \rightarrow \pi^1 K^2 \gamma$ . Starting point is a chiral Lagrangian for the pseudoscalar fields ( $\pi$  and  $K$ ) [19] where the low-lying vector mesons,  $\rho$  and  $K^*$ , are introduced via a covariant derivative leading to

$$\mathcal{L} = g_{\sigma\pi\pi} \sigma \partial_\mu \vec{\pi} \cdot \partial^\mu \vec{\pi} + g_{\rho\pi\pi} \vec{\rho}^\mu \cdot (\vec{\pi} \times \partial_\mu \vec{\pi}) + ig_{\rho KK} (\bar{K} \vec{\tau} \partial_\mu K - \partial_\mu \bar{K} \vec{\tau} K) \cdot \vec{\rho}^\mu - ig_{\pi KK^*} (\bar{K} \vec{\tau} K^{*\mu} \cdot \partial_\mu \vec{\pi} - \partial_\mu \bar{K} \vec{\tau} K^{*\mu} \cdot \vec{\pi}) + \text{h.c.} \quad (1)$$

Since we will restrict ourselves to the Born approximation, an additional (chirally invariant)  $\sigma$ - $\pi$ - $\pi$  interaction vertex with a low-mass "σ"-meson [20] has been added to adequately account for  $S$ -wave  $\pi$ - $\pi$  scattering near threshold. The corresponding Feynman diagrams, comprising  $t$ -,  $s$ -, and  $u$ -channel exchanges, are depicted in Fig. 1. The pertinent

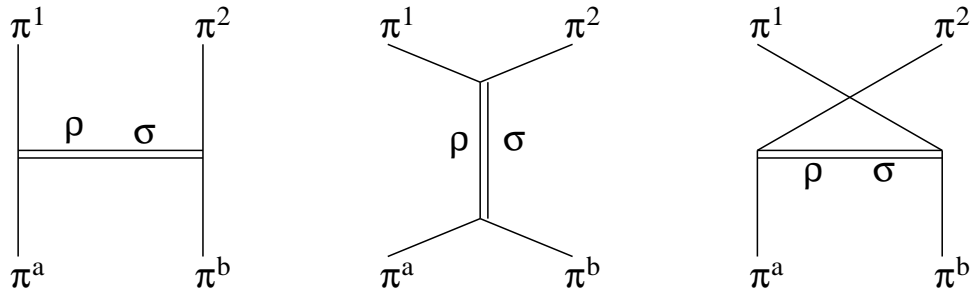


FIG. 1: Diagrams for  $\pi^a \pi^b \rightarrow \pi^1 \pi^2$  scattering.

amplitudes for elastic  $\pi^+ \pi^-$  scattering in  $t$ - and  $s$ - channel are given by

$$\begin{aligned} \mathcal{M}_t(p_a, p_b, p_1, p_2) &= \frac{-2g_{\sigma\pi\pi}^2 F^2(t)(p_a \cdot p_1)(p_b \cdot p_2)}{t - m_\sigma^2 + im_\sigma \Gamma_\sigma} + \frac{-g_{\rho\pi\pi}^2 F^2(t)(p_a \cdot p_b + p_a \cdot p_2 + p_b \cdot p_1 + p_1 \cdot p_2)}{t - m_\rho^2 + im_\rho \Gamma_\rho}, \\ \mathcal{M}_s(p_a, p_b, p_1, p_2) &= \frac{-2g_{\sigma\pi\pi}^2 (p_a \cdot p_b)(p_1 \cdot p_2)}{s - m_\sigma^2 + im_\sigma \Gamma_\sigma} + \frac{g_{\rho\pi\pi}^2 (p_a \cdot p_1 - p_a \cdot p_2 + p_b \cdot p_2 - p_b \cdot p_1)}{s - m_\rho^2 + im_\rho \Gamma_\rho}. \end{aligned} \quad (2)$$

To account for the finite size of the hadronic vertices, we introduce a momentum-transfer damping monopole form-factor,  $F(q^2)$ , for the  $t$  and  $u$  channels [7, 21],

$$F(q^2) = \frac{m_\alpha^2 - m_\pi^2}{m_\alpha^2 - q^2}, \quad (3)$$

where  $m_\alpha$  is the mass of the exchanged meson and  $q$  the four-momentum transfer (for simplicity, we neglect formfactors for  $s$ -channel polegraphs). The differential cross section for  $\pi^+ \pi^- \rightarrow \pi^+ \pi^-$  then follows as

$$\frac{d\sigma}{dt} = \frac{|\mathcal{M}_t + \mathcal{M}_s|^2}{64\pi s p_{in}^2}, \quad (4)$$

with  $p_{in} = \sqrt{(s - 4m_\pi^2)}/2$  the initial pion three-momentum in the center-of-mass frame. Fixing the parameters in the non-strange sector as in Refs. [7, 21],  $m_\sigma = 0.525$  GeV,  $\Gamma_\sigma = 0.1$  GeV,  $g_{\sigma\pi\pi} m_\sigma = 0.925$  GeV,  $m_\rho = 0.775$  GeV,

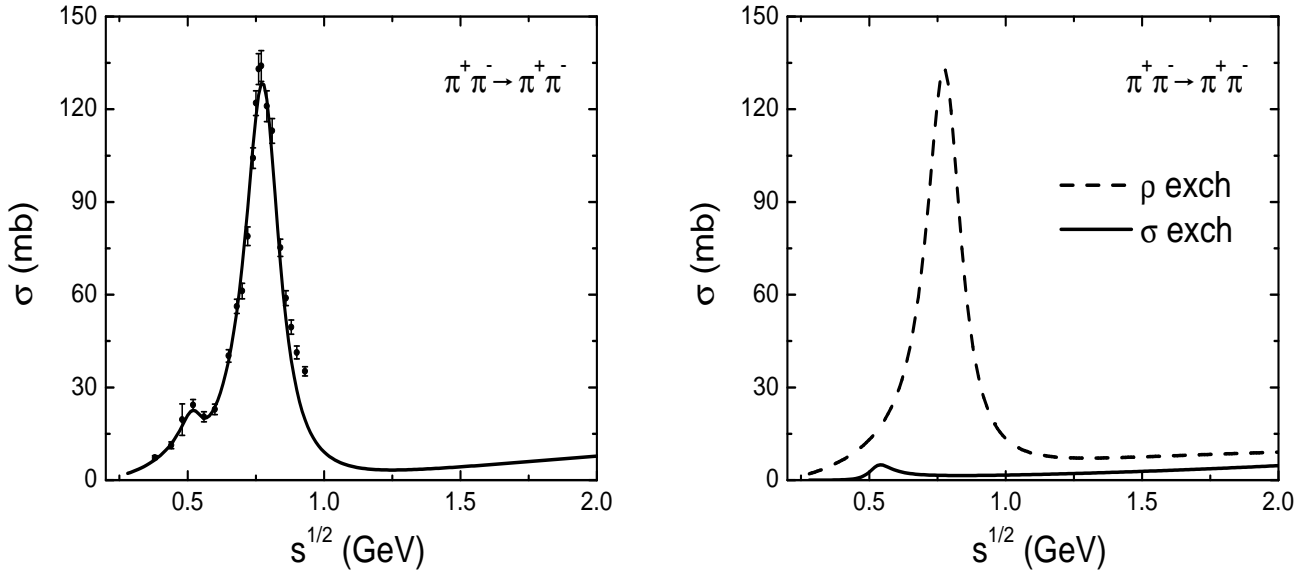


FIG. 2: Left panel: data on the elastic  $\pi^+ \pi^- \rightarrow \pi^+ \pi^-$  cross section [22] compared to a fit using a meson-exchange model in Born approximation. Right panel: decomposition of the cross section into contributions from  $\sigma$ - and  $\rho$ -exchange.

$\Gamma_\rho = 0.155$  GeV,  $g_{\rho\pi\pi} = 6.15$ , provides a fair fit to the total  $\pi\pi$  cross section [22], cf. left panel of Fig. 2. In the right panel, we display the decomposition into  $\sigma$ - and  $\rho$ -meson exchanges which identifies the  $s$ -channel  $\rho$ -polegraph as the prevalent contribution to elastic  $\pi^+ \pi^-$  scattering, while the one from  $\sigma$ -exchange is small.

Next, we turn to  $\pi$ - $K$  scattering, Bremsstrahlung off which could be significant due to both the kaon's relatively large abundance in the hadronic fireball and its resonance cross section via the  $K^*$  resonance. The relevant Feynman diagrams follow from Fig. 1 by replacing one of each in- and outgoing pion by a kaon, and the  $\rho$  by  $K^*$  (no  $\sigma$ -exchange), resulting in sixteen processes with charged particles in the initial and/or final state. The corresponding amplitudes for elastic  $\pi^-$ - $K^+$  scattering are given by

$$\begin{aligned} \mathcal{M}_t(p_a, p_b, p_1, p_2) &= \frac{-g_{\rho\pi\pi}g_{\rho KK}F^2(t)(p_a \cdot p_b + p_a \cdot p_2 + p_b \cdot p_1 + p_1 \cdot p_2)}{t - m_\rho^2 + im_\rho\Gamma_\rho} \\ \mathcal{M}_s(p_a, p_b, p_1, p_2) &= \frac{2g_{\pi KK^*}^2}{s - m_{K^*}^2 + im_{K^*}\Gamma_{K^*}} [(p_a \cdot p_1 - p_a \cdot p_2 + p_b \cdot p_2 - p_b \cdot p_1) \\ &\quad - \frac{(m_\pi^2 - m_K^2)(p_a \cdot p_1 - p_a \cdot p_2 + p_b \cdot p_1 - p_b \cdot p_2)}{m_{K^*}^2}] . \end{aligned} \quad (5)$$

As before, the hadronic  $t$ - and  $u$ -channel vertices are augmented by a formfactor,

$$F(q^2) = \frac{\Lambda^2 - m_\alpha^2}{\Lambda_\alpha^2 - q^2} , \quad (6)$$

which is of the same form as above but with a slightly different parameter dependence which facilitates a better fit to the free scattering data. Applying Eq. (4) and fixing  $\Lambda = 1.5$  GeV,  $\Gamma_{K^*} = 0.051$  GeV,  $g_{\rho KK} = g_{\pi KK^*} = 3.55$ , and  $m_{K^*} = 0.89$  GeV, the empirical cross section for elastic  $\pi^-$ - $K^+ \rightarrow \pi^-$ - $K^+$  scattering [23] is reasonably well described, cf. Fig. 3.

### III. THERMAL PHOTON EMISSION RATE

In kinetic theory, and to leading order in the e.m. coupling constant  $\alpha_{em} = 1/137$ , the thermal emission rate (per unit four-volume) of photons of energy  $q_0 = q$  for a Bremsstrahlung process of type  $a + b \rightarrow 1 + 2 + \gamma$  can be cast into the form

$$q_0 \frac{dR_\gamma}{d^3q} = N \int \frac{d^3p_a}{2E_a(2\pi)^3} \frac{d^3p_b}{2E_b(2\pi)^3} \frac{d^3p_1}{2E_1(2\pi)^3} \frac{d^3p_2}{2E_2(2\pi)^3}$$

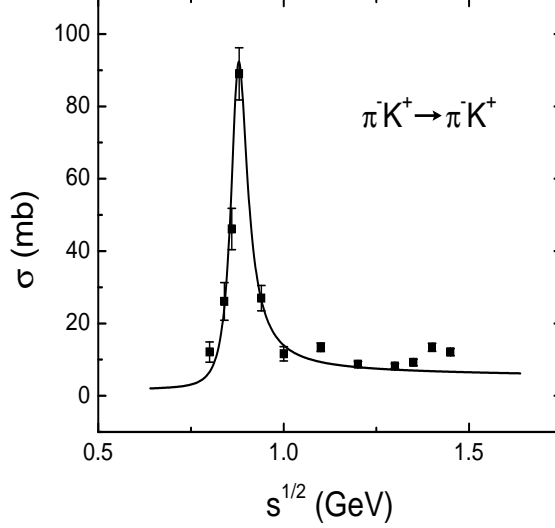


FIG. 3: Total elastic  $\pi^- K^+ \rightarrow \pi^- K$  cross section as calculated in a meson-exchange model in Born approximation compared to experimental data from Ref. [23].

$$\times (2\pi)^4 \delta^4(p_a + p_b - p_1 - p_2 - q) |\mathcal{M}_\gamma|^2 \frac{f(E_a)f(E_b)[1 \pm f(E_1)][1 \pm f(E_2)]}{2(2\pi)^3} , \quad (7)$$

where  $\mathcal{M}_\gamma$  is the corresponding scattering amplitude,  $f(E_i) = 1/(e^{(E_i - \mu_i)/T} \pm 1) \equiv f_i$  are Fermi-Dirac or Bose-Einstein distribution functions ( $\mu_i$ : chemical potential of hadron  $i$ ), and the overall degeneracy factor  $N$  depends on the specific process. As elaborated in App. A, we rewrite the emission rate without further approximation as

$$q_0 \frac{dR_\gamma}{d^3q} = \frac{N}{16(2\pi)^{11}} \int |\mathbf{p}_a| dE_a d\phi_a \int |\mathbf{p}_b| dE_b \sin\theta_b d\theta_b d\phi_b \int |\mathbf{p}_1| dE_1 \sin\theta_1 d\theta_1 d\phi_1 f_a f_b [1 + f_1][1 + f_2] \frac{|\mathcal{M}_\gamma|^2}{\mathcal{A}} \quad (8)$$

where  $\mathcal{A}$  is given as

$$\mathcal{A} = |\varphi'(\cos\theta_a^r)| \quad (9)$$

and  $\cos\theta_a^r$  is the root of the function  $\varphi(\cos\theta_a)$ ,

$$\begin{aligned} \varphi(\cos\theta_a) = & (2|\mathbf{p}_a||\mathbf{p}_b|\sin\theta_b\cos\phi_a\cos\phi_b + 2|\mathbf{p}_a||\mathbf{p}_b|\sin\theta_b\sin\phi_a\sin\phi_b - 2|\mathbf{p}_a||\mathbf{p}_1|\sin\theta_1\cos\phi_a\cos\phi_1 \\ & - 2|\mathbf{p}_a||\mathbf{p}_1|\sin\theta_1\sin\phi_a\sin\phi_1) \sqrt{1 - \cos^2\theta_a} \\ & + (2|\mathbf{p}_a||\mathbf{p}_b|\cos\theta_b - 2|\mathbf{p}_a||\mathbf{p}_1|\cos\theta_1 - 2|\mathbf{p}_a||\mathbf{q}|) \cos\theta_a \\ & + |\mathbf{p}_a|^2 + (\mathbf{p}_b - \mathbf{p}_1 - \mathbf{q})^2 - (E_a + E_b - E_1 - q_0)^2 + m_2^2 = 0. \end{aligned} \quad (10)$$

One of the main points of the present work is that the numerical evaluation of Eq. (8) goes beyond previous treatments [7, 21] by including the final state enhancement factors,  $(1 + f_1) \times (1 + f_2)$  [45], as well as for an evaluation of  $\mathcal{M}_\gamma$  beyond the soft photon approximation (SPA). The latter point is detailed in the following Section, where a summation over all possible processes for thermal photon Bremsstrahlung from  $\pi$ - $\pi$  and  $\pi$ - $K$  scattering is performed.

### A. Amplitudes for Bremsstrahlung

The photon coupling to pseudoscalar and vector mesons can be implemented via a  $U_{\text{em}}(1)$  gauge [5], rendering the interaction Lagrangian with electromagnetism as

$$\begin{aligned} \mathcal{L} = & e A^\mu (\partial_\mu \vec{\pi} \times \vec{\pi})_3 + e g_{\sigma\pi\pi} \sigma A^\mu (\partial_\mu \vec{\pi} \times \vec{\pi})_3 - e g_{\rho\pi\pi} A_\mu [\vec{\pi} \times (\vec{\pi} \times \vec{\rho}^\mu)]_3 \\ & + e \{ A^\mu (\partial_\mu \vec{\rho}' \times \vec{\rho}_\nu)_3 + [(\partial_\mu A^\nu \vec{\rho}_\nu - A^\nu \partial_\mu \vec{\rho}_\nu) \times \vec{\rho}'^\mu]_3 + [\vec{\rho}'^\mu \times (A^\nu \partial_\mu \vec{\rho}_\nu - \partial_\mu A^\nu \vec{\rho}_\nu)]_3 \} \end{aligned}$$

$$\begin{aligned}
& +ie[A^\mu(\bar{K}^{*\nu}Q\partial_\mu K_\nu^* - \partial_\mu\bar{K}^{*\nu}QK_\nu^*) + \bar{K}^{*\mu}Q(\partial_\mu A^\nu K_\nu^* - A^\nu\partial_\mu K_\nu^*) + (A^\nu\partial_\mu\bar{K}_\nu^* - \partial A^\nu\bar{K}_\nu^*)QK^{*\mu}] \\
& +ieA^\mu(\bar{K}Q\partial_\mu K - \partial_\mu\bar{K}QK) - eg_{\pi KK^*}A^\mu[\bar{K}^*(2\vec{\tau}Q - Q\vec{\tau})K + \bar{K}(2Q\vec{\tau} - \vec{\tau}Q)K^*] \cdot \vec{\pi} \\
& +eg_{\rho KK}A^\mu\bar{K}(\vec{\tau}Q + Q\vec{\tau})K \cdot \vec{\rho}_\mu,
\end{aligned} \tag{11}$$

where  $A^\mu$  is the electromagnetic field,  $Q = \text{diag}(1, 0)$  the charge operator, and the subscript “3” denotes the third component of isospin.

First, we consider the process for Bremsstrahlung of a photon via  $\pi^a\pi^b \rightarrow \pi^1\pi^2\gamma$  scattering, based on the diagrams depicted in Fig. 1. In charge basis, this amounts to the following seven processes:  $\pi^+\pi^- \rightarrow \pi^+\pi^-(\pi^0\pi^0)$ ,  $\pi^+\pi^0 \rightarrow \pi^+\pi^0$ ,  $\pi^-\pi^0 \rightarrow \pi^-\pi^0$ ,  $\pi^0\pi^0 \rightarrow \pi^+\pi^-$ ,  $\pi^+\pi^+ \rightarrow \pi^+\pi^+$ , and  $\pi^-\pi^- \rightarrow \pi^-\pi^-$ , with a photon attached to each external or internal charged particle. E.g., the amplitude for the process  $\pi^+\pi^- \rightarrow \pi^+\pi^-\gamma$  with a photon attached to a charged external pion in all possible ways reads

$$\begin{aligned}
\mathcal{M}^\mu = & eJ_a^\mu[\mathcal{M}_t(p_a - q, p_b, p_1, p_2) + \mathcal{M}_s(p_a - q, p_b, p_1, p_2)] \\
& +eJ_b^\mu[\mathcal{M}_t(p_a, p_b - q, p_1, p_2) + \mathcal{M}_s(p_a, p_b - q, p_1, p_2)] \\
& +eJ_1^\mu[\mathcal{M}_t(p_a, p_b, p_1 + q, p_2) + \mathcal{M}_s(p_a, p_b, p_1 + q, p_2)] \\
& +eJ_2^\mu[\mathcal{M}_t(p_a, p_b, p_1, p_2 + q) + \mathcal{M}_s(p_a, p_b, p_1, p_2 + q)],
\end{aligned} \tag{12}$$

where  $\mathcal{M}_s$  and  $\mathcal{M}_t$  are the amplitudes quoted in Sec. II. In the above,

$$J_{a,b}^\mu = \frac{-Q_{a,b}(2p_{a,b} - q)^\mu}{2p_{a,b} \cdot q}, \quad J_{1,2}^\mu = \frac{Q_{1,2}(2p_{1,2} + q)^\mu}{2p_{1,2} \cdot q} \tag{13}$$

are the electromagnetic currents with  $Q_i$  the charge of the pion in units of the proton charge. Electromagnetic gauge invariance furthermore requires the incorporation of contact diagrams with the photon attached to each proper vertex. In App. B we explicitly construct the pertinent amplitudes so that the total satisfies  $q_\mu \cdot \mathcal{M}^\mu = 0$ . For the processes with four-point vertices one arrives at

$$\begin{aligned}
\mathcal{M}_c^\mu = & \frac{2eg_{\sigma\pi\pi}^2 F[(p_b - p_2)^2](p_a + p_1)^\mu p_b \cdot p_2}{(p_b - p_2)^2 - m_\sigma^2 + im_\sigma\Gamma_\sigma} - \frac{2eg_{\sigma\pi\pi}^2 F[(p_a - p_1)^2]p_a \cdot p_1(p_b + p_2)^\mu}{(p_a - p_1)^2 - m_\sigma^2 + im_\sigma\Gamma_\sigma} \\
& - \frac{2eg_{\sigma\pi\pi}^2 (p_a - p_b)^\mu p_1 \cdot p_2}{(p_1 + p_2)^2 - m_\sigma^2 + im_\sigma\Gamma_\sigma} - \frac{2eg_{\sigma\pi\pi}^2 p_a \cdot p_b(p_1 - p_2)^\mu}{(p_a + p_b)^2 - m_\sigma^2 + im_\sigma\Gamma_\sigma} \\
& - \frac{2eg_{\rho\pi\pi}^2 F[(p_a - p_1)^2](p_a + p_1)^\mu}{(p_a - p_1)^2 - m_\rho^2 + im_\rho\Gamma_\rho} + \frac{2eg_{\rho\pi\pi}^2 F[(p_b - p_2)^2](p_b + p_2)^\mu}{(p_b - p_2)^2 - m_\rho^2 + im_\rho\Gamma_\rho} \\
& - \frac{2eg_{\rho\pi\pi}^2 (p_a - p_b)^\mu}{(p_a + p_b)^2 - m_\rho^2 + im_\rho\Gamma_\rho} - \frac{2eg_{\rho\pi\pi}^2 (p_1 - p_2)^\mu}{(p_1 + p_2)^2 - m_\rho^2 + im_\rho\Gamma_\rho}.
\end{aligned} \tag{14}$$

The same procedure of deriving the Bremsstrahlung amplitude, leading to Eqs. (12), can be applied to  $\pi\text{-}K$  scattering. The additional contact terms necessary to maintain gauge invariance are given by

$$\begin{aligned}
\mathcal{M}_c^\mu = & -\frac{2eg_{\rho\pi\pi}g_{\rho KK}F[(p_a - p_1)^2](p_a + p_1)^\mu}{(p_a - p_1)^2 - m_\rho^2 + im_\rho\Gamma_\rho} + \frac{2eg_{\rho\pi\pi}g_{\rho KK}F[(p_b - p_2)^2](p_b + p_2)^\mu}{(p_b - p_2)^2 - m_\rho^2 + im_\rho\Gamma_\rho} \\
& -\frac{4eg_{\pi KK^*}^2[(p_a - p_b)^\mu - (m_a^2 - m_b^2)(p_a + p_b)^\mu/m_{K^*}^2]}{(p_a + p_b)^2 - m_{K^*}^2 + im_{K^*}\Gamma_{K^*}} \\
& -\frac{4eg_{\pi KK^*}^2[(p_1 - p_2)^\mu - (m_1^2 - m_2^2)(p_1 + p_2)^\mu/m_{K^*}^2]}{(p_1 + p_2)^2 - m_{K^*}^2 + im_{K^*}\Gamma_{K^*}},
\end{aligned} \tag{15}$$

which completes the set of processes for  $\pi K \rightarrow \pi K\gamma$ .

## B. Soft Photon Emission Rates

With the amplitudes as specified in the previous section we now proceed to the results of the numerical integration of the thermal photon production rate, Eq. (8). In Fig. 4 we compare our new results for Bremsstrahlung off  $\pi\text{-}\pi$  scattering to earlier calculations. With the application to URHICs in mind, we choose medium conditions representing  $Pb\text{-}Pb$  collisions at full SPS energy, roughly half way through the hadronic evolution, corresponding to a temperature

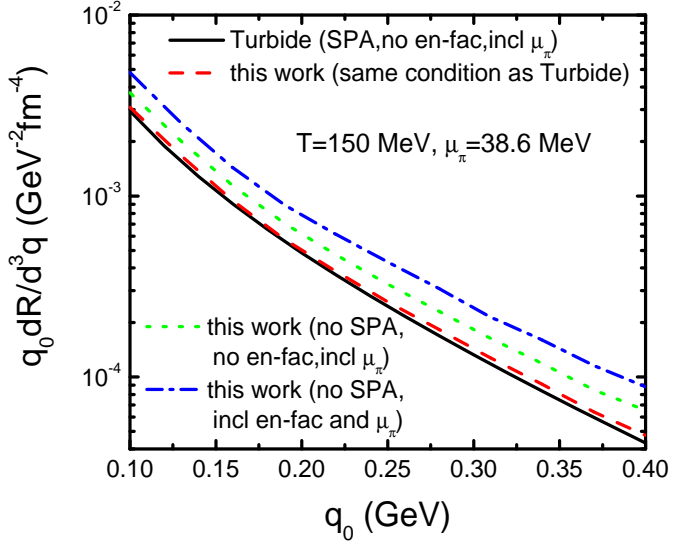


FIG. 4: Comparison of various approximations to the thermal photon rate for  $\pi\pi \rightarrow \pi\pi\gamma$  reactions as a function of photon energy.

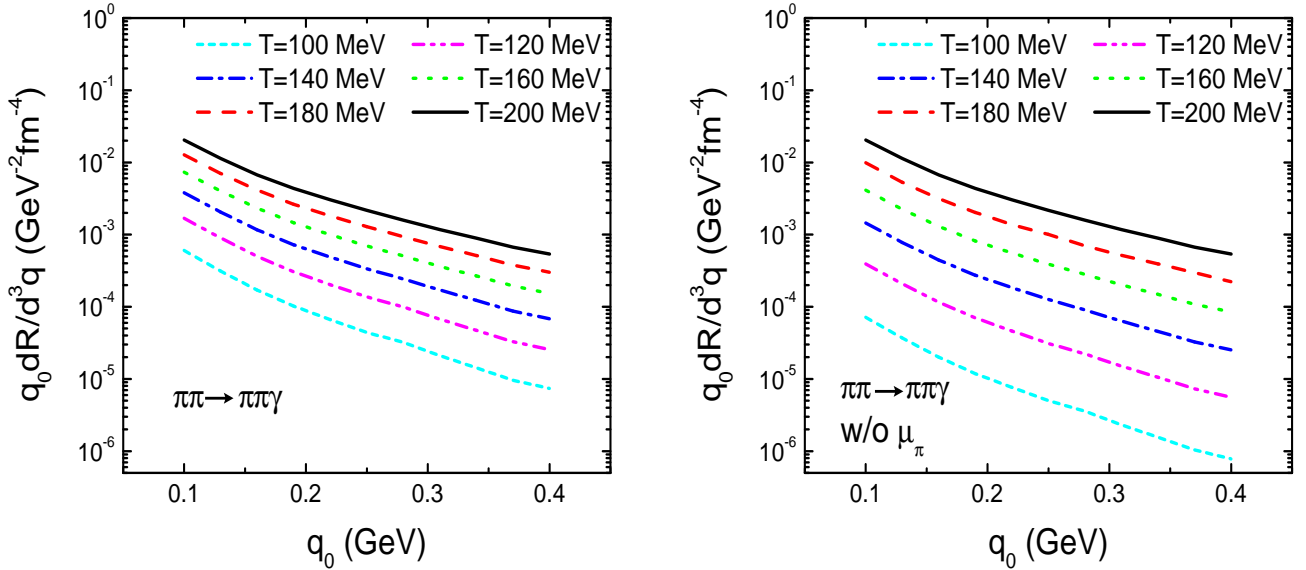


FIG. 5: Thermal photon emission rate from Bremsstrahlung via  $\pi\pi \rightarrow \pi\pi\gamma$  reactions as a function of photon energy at different temperatures. The left panel includes pion chemical potentials appropriate for  $Pb(158 \text{ AGeV})-Pb$  collisions while in the right panel  $\mu_\pi = 0$ .

of  $T = 150$  MeV and a pion chemical potential of  $\mu_\pi \simeq 40$  MeV [9, 25]. When working in the soft photon approximation (SPA) and neglecting final-state Bose enhancement factors for the outgoing pions, our results closely coincide with computations by Turbide et al. [13, 14] (dashed vs. solid line in Fig. 4). When the SPA is relaxed, the rate is found to increase by about 25% at low energies ( $q_0 = 0.1$  GeV) and close to 40% at higher energies ( $q_0 \simeq 0.4$  GeV), see the short-dashed line in Fig. 4. Finally, when implementing the final-state Bose enhancement, the rate rises another  $\sim 30\%$ . Thus, the total increase of soft photon emission over previous computations amounts to 60-100%, which is quite appreciable.

In Fig. 5 we display the temperature evolution of the Bremsstrahlung rate from  $\pi\pi$  scattering. The left panel includes pion-chemical potentials as estimated in Ref. [25] to preserve the pion (and kaon) number in the hadronic evolution of  $Pb-Pb$  collisions after chemical freezeout, parametrized by a linear increase with temperature ( $T$  in units

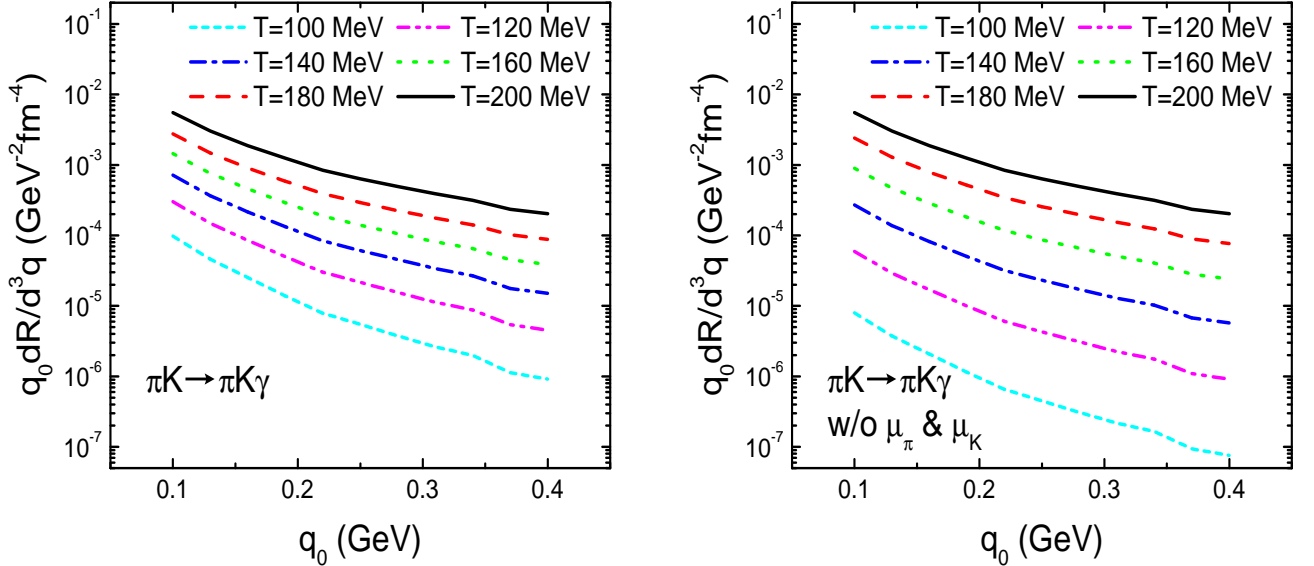


FIG. 6: Thermal photon Bremsstrahlung emission rate from  $\pi K \rightarrow \pi K\gamma$  reactions as a function of photon energy at different temperatures.

of GeV),

$$\mu_\pi = \frac{0.2 - T}{1.05} \text{ GeV} , \quad \mu_K = 1.9(0.175 - T) \text{ GeV} \quad (16)$$

(a small nonvanishing value of  $\mu_\pi$  at chemical freezeout has been introduced to reproduce the measured pion-to-baryon ratio at full SPS energy; this is due to the somewhat limited number of resonances included in the equation of state in Ref. [25] which affects the pion yield via feeddown; it slightly overestimates (underestimates) the direct pion density at large (small) temperature, e.g.,  $e^{\mu_\pi/T} = 1.11$  at  $T = 0.18$  GeV). When reducing the temperature from  $T = 0.18$  GeV to  $0.11$  GeV, the decrease in rate is close to a factor of 10 at  $q_0 = 0.1$  GeV but becomes a factor of  $\sim 15$  at  $q_0 = 0.4$  GeV, reflecting the larger slope at smaller  $T$ . This also entails an increasing weight of photon emission at lower energies toward later stages in the fireball evolution (note that increase in the hadronic fireball volume between chemical ( $T_c = 0.175$  GeV) and thermal freezeout ( $T = 0.110$  GeV) is about a factor of  $\sim 6$ , implying that the yield of Bremsstrahlung photons is rather sensitive to the (later stages) of the fireball lifetime). In the right panel of Fig. 5, the pion-chemical potentials are set to zero: the decrease compared to the  $\mu_\pi \neq 0$  results amounts to slightly more than a fugacity factor squared,  $e^{2\mu_\pi/T}$  (as one would naively expect for  $\pi\pi$  annihilation), mostly due to the final-state enhancement factors. Finally, a comparison to the hadronic rate calculations of Ref. [9] reveals that  $\pi\pi$  Bremsstrahlung as computed here exceeds previously dominant baryonic contributions by close to a factor of 2 at  $q_0 = 0.2$  GeV, and is smaller by a factor of 2 at  $q_0 = 0.4$  GeV.

Turning to  $\gamma$  radiation off (elastic)  $\pi$ - $K$  scattering (Fig. 6), we find the emission rate to be at the  $\sim 20\%$  level of the one from  $\pi\pi$  scattering, which essentially reflects the experimentally observed  $K/\pi$  ratio. Since  $\pi\pi$  scattering will provide the dominant contribution to the overall low-energy yield (i.e., in the low- $q_t$  spectra of URHICs), the strangeness component is not insignificant. Also, the role of the kaon-chemical potential,  $\mu_K$ , is equally relevant for maintaining a substantial emission rate for  $\pi$ - $K$  scattering toward lower temperatures (compare left and right panels of Fig. 6) as is  $\mu_\pi$  for  $\pi\pi$  scattering.

#### IV. LANDAU-POMERANCHUK-MIGDAL EFFECT

When the formation time of the emitted photon,  $\tau_{form} \sim 1/q_0$ , becomes of the same order as the time between subsequent  $\pi\pi$  collisions,  $\tau_\pi^{coll}$ , coherence effects are expected to become important (Landau-Pomeranchuk-Migdal (LPM) effect [26]). For soft photon and dilepton production in a dense hadronic gas, the LPM interference has been studied in Refs. [6, 17, 18]. Here, we put these estimates into quantitative context with our updated rate calculations. First, we employ the expression derived in Ref. [17], where the LPM effect was implemented in SPA resulting in a

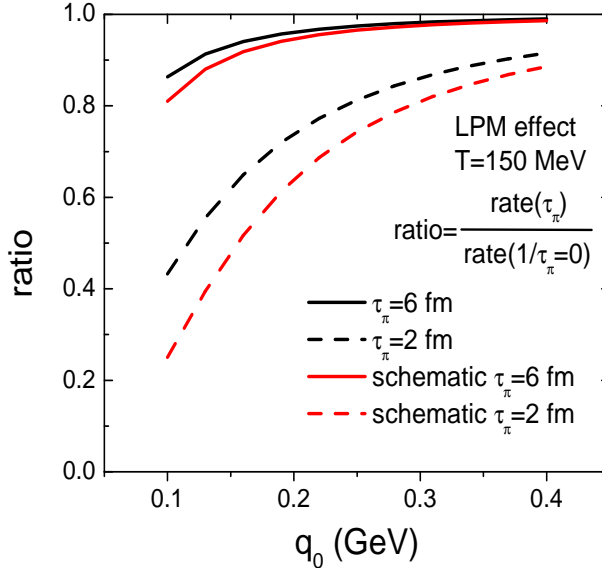


FIG. 7: Influence of the LPM effect on thermal photon bremsstrahlung from  $\pi\pi$  scattering at  $T = 150$  MeV.

differential cross section of photon production off  $\pi\pi$  scattering as

$$q_0 \left\langle \frac{d\sigma^\gamma}{d^3q} \right\rangle = \sigma_{\pi\pi} \frac{2\alpha}{(2\pi)^2} \left\langle v^2 \frac{(1 - \cos^2\theta)}{a^2 + q_0^2(1 - v\cos\theta)^2} \right\rangle. \quad (17)$$

$\langle \cdot \rangle$  indicates averaging over the time between successive collisions and over all the velocities after the collision (for simplicity, we choose an average velocity  $v = 0.5c$ ),  $\sigma_{\pi\pi}$  denotes the elastic  $\pi\pi$  cross section (which factorizes in SPA) and  $1/a = \tau_\pi^{coll} = 1/\Gamma_\pi$  is the pion collision time (or inverse scattering width). The latter, in turn, depends on the hadron densities and pertinent pion cross sections, schematically given by

$$\Gamma_\pi = \sum_h n_h(T, \mu_h) \sigma_{\pi h} v_{rel}, \quad (18)$$

where the summation is, in principle, over all hadrons in the heat bath ( $h = \pi, K, N, \Delta, \dots$ ;  $v_{rel}$ : relative velocity between  $\pi$  and  $h$ ). For a selfconsistently calculated pion gas at  $(T, \mu_\pi) = (150, 0)$  MeV with realistic  $\pi\pi$  interactions [27], one finds  $\tau_\pi^{coll} \simeq 6$  fm/c, while a hot  $\pi N \Delta$  gas representative for SPS conditions leads to  $\tau_\pi^{coll} \simeq 2$  fm/c [28]. In Fig. 7 we used both values to bracket the uncertainty in the suppression of low-energy photons, by plotting the ratio of Eq. (17) to the incoherent limit ( $a = 0$ ). For  $\tau_\pi^{coll} = 6$  fm/c, the quenching factor is rather small reducing the photon emission rate by no more than 15% even at the smallest energies considered here,  $q_0 = 100$  MeV. This is consistent with Ref. [18] where a slightly different coherence factor has been derived, amounting to a multiplication of the incoherent rate by  $[(q_0\tau)^2/(1 + (q_0\tau)^2)]^2$ ; for  $\tau_\pi^{coll} = 6$  fm/c and  $q_0 = 100$  MeV the latter turns out to be 0.81. However, for  $\tau_\pi^{coll} = 2$  fm/c and  $q_0 = 100$  MeV, collision and formation time are of comparable magnitude, and the quenching factor becomes substantial, between 0.4 and 0.25 according to the two ways of estimating it.

## V. SCHEMATIC ESTIMATE OF MEDIUM EFFECTS

When hadrons are embedded into a hot and dense medium, their vacuum properties (mass and width) are expected to change, which is encoded in pertinent spectral functions,

$$A_h(k_0, k) = -2 \operatorname{Im} D_h(k^2) = -2 \operatorname{Im} \left( \frac{1}{k^2 - m_h^2 - \Sigma_h(k_0, k)} \right), \quad (19)$$

where  $\Sigma_h(k_0, k)$  is the self-energy of meson  $h$  as induced by interactions with the surrounding matter particles. For the present purpose, the relevant mesons are the  $\rho$  and the “ $\sigma$ ” which figure into the meson-exchange propagators in the amplitudes (since we work in Born approximation, no explicit pion propagators appear). Dilepton spectra in heavy-ion collisions have revealed ample evidence that the in-medium  $\rho$ -meson spectral function is substantially modified. While

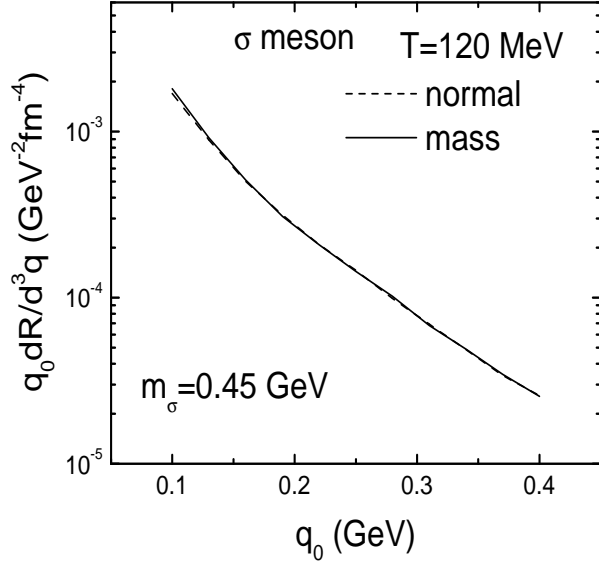


FIG. 8: In-medium effects on thermal photon production implemented by a dropping “ $\sigma$ ”-meson mass in Bremsstrahlung off  $\pi$ - $\pi$  scattering. Dashed ( $m_\sigma = 0.525$  GeV) and solid line ( $m_\sigma = 0.45$  GeV) are almost indistinguishable due to the minor role of “ $\sigma$ ”-exchange in the total elastic  $\pi$ - $\pi$  cross section at low energy.

the low-mass enhancement observed by CERES/NA45 in  $Pb(158\text{ AGeV})$ - $Au$  collisions [29] is compatible with both the assumption of a dropping  $\rho$ -mass and a broadening as predicted by hadronic many-body theory [25], more recent NA60 dimuon spectra [30] clearly favor the latter [31]. Concerning the “ $\sigma$ ” meson, 2-pion production experiments off nuclei [32, 33] indicate substantial medium effects as well, in terms of an enhancement near the two-pion threshold which increases with nuclear mass number  $A$ . Whether this is due to a dropping “ $\sigma$ ”-meson mass [34] or hadronic many-body effects [35] (or both), is not clear at present. At finite temperature, the (the approach to) chiral symmetry restoration (implying degeneracy of  $\pi$ - and  $\sigma$ - spectral functions), is suggestive for a  $\sigma$ -mass approaching the pion mass [36]. It is therefore desirable to investigate to what extent Bremsstrahlung off  $\pi$ - $\pi$  scattering is sensitive to modifications of “ $\sigma$ ” and  $\rho$  mesons. Previous studies along these lines [37, 38, 39] have mostly addressed hadronic photon emission at higher energies (in connection with a dropping  $\rho$  mass).

In light of the above, we here focus on the effects of a reduced  $\sigma$ -mass on low-energy photon emission. We will not address changes in the  $\rho$ -meson properties, as a simple dropping mass appears to be ruled out while a consistent implementation of changes in the width in the propagator requires accounting for the pertinent processes in the photon production rate as well (for the same reason, we do not consider width changes in the  $\sigma$ -propagator).

When recalculating photon Bremsstrahlung off  $\pi$ - $\pi$  scattering by reducing the mass of the  $\sigma$  meson to  $m_\sigma = 0.45$  GeV (as compared to 0.525 GeV before), the thermal emission rate barely changes, cf. Fig. 8. This can be readily understood by recalling the elastic  $\pi$ - $\pi$  cross section, see right panel in Fig. 2, where the  $\sigma$ -meson contribution plays a minor role; nevertheless, the smallness of the effect when dropping the  $\sigma$ -mass by  $\sim 15\%$  is not necessarily expected, but forces us to conclude that low-energy thermal photon spectra are not sensitive to (partial) chiral symmetry restoration in the scalar channel (for completeness we state that the rate of low-energy photon production increases by  $\sim 25\%$  if one were to reduce the  $\rho$ -meson mass from its vacuum value of 0.77 GeV to 0.65 GeV).

## VI. PHOTON SPECTRA IN HEAVY-ION COLLISIONS

We now apply our Bremsstrahlung rates to the calculation of photon spectra at low transverse momentum in central  $Pb(158\text{ AGeV})$ - $Pb$  collisions at SPS. We supplement the spectra with the baseline results of Ref. [9] and compare the total to the recent WA98 data [12]. As in Ref. [9], the folding of the thermal emission rates over the space-time evolution is performed with the help of an expanding fireball evolution which has been parametrized to reflect basic features of hydrodynamic models. With a hadronic resonance-gas equation of state (with chemical freezeout at  $(\mu_N^{ch}, T_{ch}) = (250, 175)$  MeV) and a participant-nucleon number of  $N_{part} = 340$  to represent the 10% most central collisions, the fireball volume at chemical freezeout is fixed to approximately reproduce the observed hadron

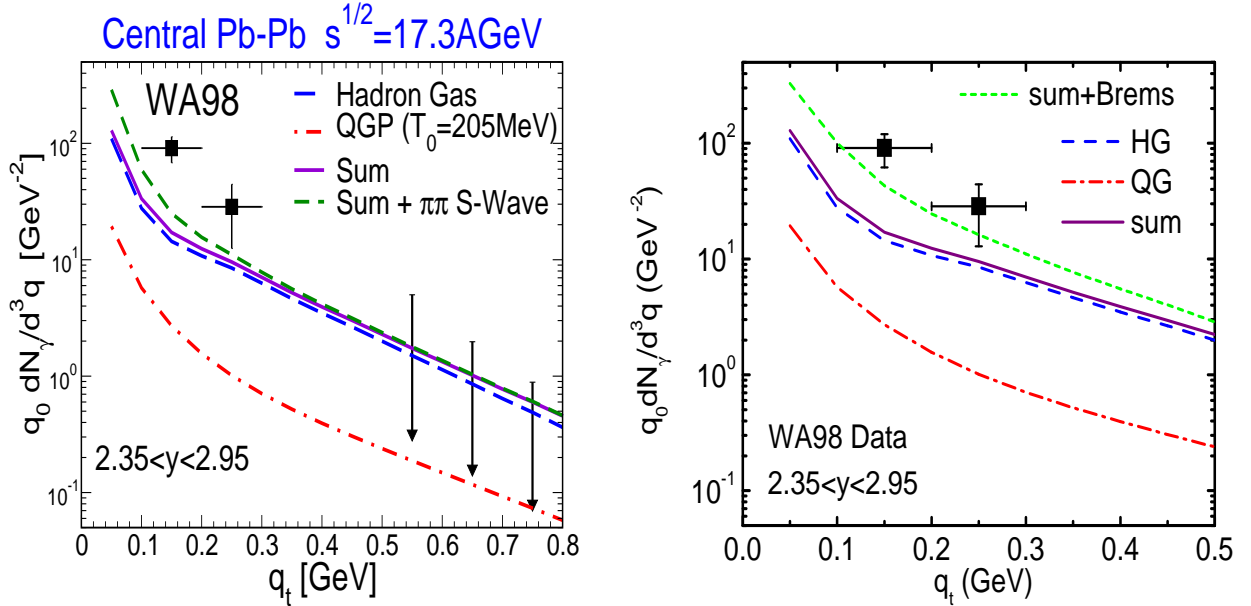


FIG. 9: Direct low- $q_t$  photon spectra as measured in central  $Pb-Pb$  collisions at SPS [12] compared to thermal emission spectra from an expanding thermal fireball with QGP and hadronic phases [9]. In the left panel (taken from Refs. [13, 14]) QGP [40] (dash-dotted line) and hadron gas (HG) emission [9] (dashed line, without meson-meson Bremsstrahlung) add up to the solid line, while the upper dashed line additionally includes an estimate [13] of Bremsstrahlung off  $\pi\pi$  scattering in the soft-photon approximation (SPA) and without final-state Bose enhancement factors, representing the rate depicted by the solid line in Fig. 4 (the contributions from  $\rho \rightarrow \pi\pi\gamma$  decays in the HG rates of Ref. [9] have been removed to avoid double counting). The downward arrows represent 90% upper confidence limits set by WA98 in an earlier measurement [11]. The curves in the right panel are as in the left panel except that the upper dashed line now includes the improved rates from elastic  $\pi\pi$  and  $\pi K$  Bremsstrahlung (without SPA, including final-state Bose enhancement and with the same caveat on double counting as in the left panel).

multiplicities (after chemical freezeout, the evolution is constructed using entropy and baryon-number conservation, as well as meson-chemical potentials to preserve the correct hadron ratios). After averaging over the appropriate rapidity interval of the WA98 acceptance the thermal photon spectra follow as

$$q_0 \frac{dN}{d^3q}(q_t) = \frac{1}{\Delta y} \int_{y_{min}}^{y_{max}} dy \int d\tau V_{FB}(\tau) q_0 \frac{dR^\gamma}{d^3q} \quad (20)$$

with  $y_{min} = 2.35$  and  $y_{max} = 2.95$  ( $\Delta y = 0.6$ ). The fireball volume is taken to evolve with proper time as

$$V_{FB}(\tau) = \frac{1}{2} \pi (z_0 + v_{z,0}\tau + \frac{1}{2} a_z \tau^2) (r_{T,0} + \frac{1}{2} a_T \tau^2)^2 \quad (21)$$

with  $z_0 = 1.8$  fm (corresponding to a formation time of 1 fm/c and translating into an average initial temperature of  $T_0 = 205$  MeV),  $r_{T,0} = 6.25$  fm,  $a_z = a_T = 0.045$  fm $^2$ /fm, and  $v_z = 0.6c$  (note that only half of the total fireball volume must be used to reproduce the correct  $dN_{ch}/dy$ ). QGP and mixed phase are completed after  $\tau_H \simeq 4.46$  fm/c and thermal freezeout is assumed at  $\tau_{fo} = 13$  fm/c (plus one extra fm/c to allow for strong resonance decays). The numerically inferred temperature evolution in the hadronic phase can be conveniently parametrized as

$$T(\tau) = \frac{1}{c_1 + c_2 R(\tau)} \text{GeV} \quad (22)$$

with  $c_1 = 1.3$ ,  $c_2 = 0.639$  fm, and a “radius”

$$R(\tau) = \left( \frac{3}{4\pi} V_{FB}(\tau) \right)^{\frac{1}{3}} \quad (23)$$

Parameterizations of the numerically computed Bremsstrahlung rates along the temperature-chemical potential trajectory used here are quoted in App. C.

In Fig. 9 we summarize our results for direct photon spectra in central  $Pb(158 \text{ AGeV})-Pb$  in comparison to the low- $q_t$  data of the WA98 collaboration [12] at the CERN-SPS. The left panel reproduces the previous calculations for QGP and hadron gas emission of Ref. [9] (lower three curves), which are in good agreement with earlier WA98 spectra at  $q_t \geq 1.5 \text{ GeV}$ , but significantly underestimate the low-momentum data at  $q_t = 0.1 - 0.3 \text{ GeV}$ . This is still true upon inclusion of Bremsstrahlung off  $\pi\pi$  scattering [13, 14] (treated in SPA and without final-state Bose enhancement), even though this contribution is noticeable. However, if the improved Bremsstrahlung rates from  $\pi\pi$  and  $\pi K$  interactions are employed, the discrepancy is reduced appreciably, resulting in approximate agreement with experiment, see right panel of Fig. 9 (note that the Bremsstrahlung yield decreases faster with energy than the other hadronic contributions, thereby not upsetting the agreement of the previous calculations with the experimental spectra (upper limits) at higher energies). These findings are presumably to be considered as an upper limit since at this point we do not account for LPM suppression effects as discussed in Sec. IV. The thermal low- $q_t$  photon yield is furthermore found to approximately scale with the fireball lifetime, which reiterates the importance of the later hadronic stages.

We also note that baryon-induced effects, which enter through a medium modified  $\rho$  spectral function [25] carried to the photon point and which dominate the contribution labelled ‘‘HG’’ at the depicted momenta, are appreciable (at the 30-60% level in the range  $q_t = 0.1 - 0.3 \text{ GeV}$ ). Besides resonance decays (e.g.,  $\Delta, N(1520) \rightarrow N\gamma$ ), these include Bremsstrahlung from  $\pi-N$ ,  $N-N$ , and  $N-\Delta$  interactions (as following from  $\pi NN^{-1}$  and  $\pi\Delta N^{-1}$  excitations in the pion cloud of the  $\rho$ -meson), which have been constrained by (the inverse process of) photoabsorption on the nucleon and nuclei [41]. In Ref. [8], similar contributions were claimed to be smaller.

## VII. COHERENT EMISSION FROM HEAVY-ION COLLISIONS

Another source of soft direct photons in heavy-ion collisions that we would like to study here is (nonthermal) Bremsstrahlung emission due to coherent radiation off the protons within the incoming nuclei [42, 43]. In the long-wave length limit,  $\lambda_\gamma = 2\pi/q \gg D$  ( $q$ : photon 3-momentum,  $D \simeq 10 \text{ fm}$ : typical system size), phase interferences are suppressed and the radiation can be assessed via the rapidity shift that the protons undergo from the initial nuclei to the finally observed distribution. Including both target and projectile, and for central collisions, one finds the following form of the photon spectrum [42, 43],

$$q_0 \frac{dN_\gamma}{d^3q} = \frac{\alpha_{em}}{4\pi^2 q_0^2} \left| \int dy \left\{ \frac{dN}{dy} \Big|_P \left[ \frac{v\sin\theta}{1-v\cos\theta} - \frac{v_P\sin\theta}{1-v_P\cos\theta} \right] + \frac{dN}{dy} \Big|_T \frac{v\sin\theta}{1-v\cos\theta} \right\} \right|^2 \quad (24)$$

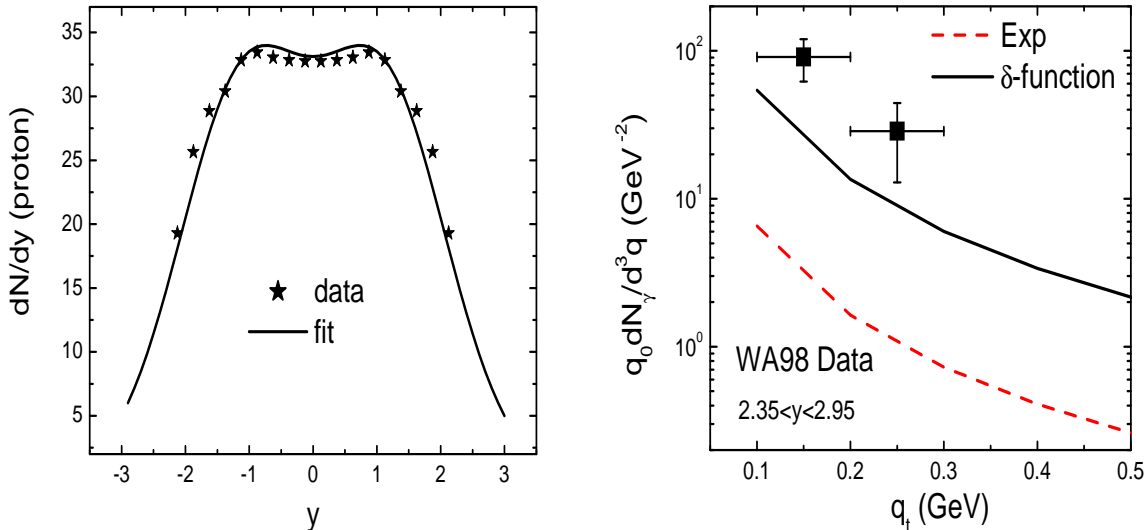


FIG. 10: Left panel: two-Gaussian fit (with centers at  $y_0 = \pm 1.1$  and width  $\sigma_y = 1.0$ ) to the experimental proton rapidity distributions [44] in central  $Pb(158 \text{ AGeV})-Pb$ . Right panel: coherent photon spectra from  $Pb-Pb$  collisions at SPS using final-state proton rapidity distributions from experiment (dashed line) or  $\delta$ -functions centered at  $y_{P,T} = \pm 0$  (solid line), compared to the experimental data [12].

where  $v_P$  is the beam velocity,  $y = \tanh^{-1} v$  is the final-state (FS) proton rapidity, and

$$\left. \frac{dN}{dy} \right|_P \quad \text{and} \quad \left. \frac{dN}{dy} \right|_T \quad (25)$$

are the pertinent FS rapidity distributions for projectile and target nuclei, respectively. The latter can be reasonably well fitted to experimental data [44] using two Gaussians, cf. left panel of Fig. 10. In the right panel of Fig. 10 we summarize our results for coherent emission from the longitudinal deceleration of the incoming protons. With realistic final rapidity distributions (dashed line) the photon yield is well below 10% of the WA98 low-energy data, which presumably is an upper limit since already for  $q_0 = 0.1$  GeV, the pertinent photon wavelength,  $\lambda_\gamma \simeq 12$  fm, is of the order of the system size rendering phase variations (interference) potentially relevant. Even with the extreme assumption of  $\delta$ -function like proton rapidity distributions at  $y_{P,T} = 0$  (full stopping), the coherent emission yield falls short of the data. We thus conclude that the latter cannot be at the origin of the observed enhancement of previous predictions [9].

## VIII. SUMMARY AND DISCUSSION

In this article we have revisited the problem of soft photon production in ultrarelativistic heavy-ion collision which has recently received renewed interest by the observation of a large excess by the WA98 collaboration in central  $Pb$ - $Pb$  collisions at the CERN-SPS. Earlier predictions using two-body mesonic and baryon-induced thermal photon production significantly underestimated these data. We have thus focused on a more elaborate re-evaluation of Bremsstrahlung from meson-meson interactions. Based on a  $U_{\text{em}}(1)$ -gauged meson-exchange model for elastic  $\pi$ - $\pi$  and  $\pi$ - $K$  scattering (in Born approximation), our main improvement over previous calculations consists of a full numerical treatment of the collision integral which goes beyond the commonly employed soft-photon approximation and allows for the inclusion of final-state Bose enhancement factors. We have explicitly constructed pertinent contact interactions to preserve electromagnetic gauge invariance of the underlying Bremsstrahlung amplitude. The combined effect of the two improvements amounts to an increase of the thermal  $\pi$ - $\pi$  Bremsstrahlung rate by up to a factor of 2 at low photon energies ( $q_0 = 0.1 - 0.5$  GeV), while  $\pi$ - $K$  scattering adds another  $\sim 20\%$  (essentially reflecting the  $K/\pi$  ratio in the hadronic gas). As a consequence, meson-meson Bremsstrahlung becomes the dominant thermal photon source at low energies. When combined with previous rate calculations, the convolution over a standard thermal fireball evolution leads to approximate agreement with the low-momentum WA98 data. This comparison, however, does not include the LPM effect, which we have estimated to suppress the emission rate by up to several tens of percent. We have furthermore shown that the Bremsstrahlung rates are rather insensitive to medium effects on the “ $\sigma$ ”-meson in form of a reduced mass, due to the fact that the elastic  $\pi$ - $\pi$  cross section is dominated by ( $s$ -channel)  $\rho$  exchange. We finally studied the possibility of coherent Bremsstrahlung induced by rapidity shifts of the incoming projectile and target protons. When using realistic final-state distributions, we have found this contribution to be essentially negligible.

While our investigations suggest that thermal emission from hadronic matter is at the origin of the low- $q_t$  WA98 enhancement, more work is required to quantify the theoretical estimates, e.g. by merging medium effects on the  $\rho$ -meson (as implicit in rate estimates using in-medium spectral functions) with the newly computed Bremsstrahlung rates, as well as by a more accurate treatment of the LPM effect. In addition, an experimental confirmation of the observed enhancement, e.g. at the Relativistic Heavy-Ion Collider (RHIC), would be very illuminating.

### Acknowledgments

We gratefully acknowledge discussions with C. Gale and S. Turbide in the early stages of this work, and for supplying us with the Bremsstrahlung rates used in the left panel of Fig. 9. We also wish to thank Che-Ming Ko and Hendrik van Hees for helpful discussions. This work was supported in part by a U.S. National Science Foundation CAREER award under grant PHY-0449489.

## APPENDIX A: EVALUATION OF THE BREMSSTRAHLUNG PHASE SPACE INTEGRAL

In this appendix, we derive the expressions for the photon emission rate as used in Sec. III. Starting from the kinetic theory expression, Eq. (7) in the main text, for  $\pi + \pi \rightarrow \pi + \pi + \gamma$ ,

$$q_0 \frac{dR^\gamma}{d^3q} = N \int \frac{d^3p_a}{2E_a(2\pi)^3} \frac{d^3p_b}{2E_b(2\pi)^3} \frac{d^3p_1}{2E_1(2\pi)^3} \frac{d^3p_2}{2E_2(2\pi)^3} \times (2\pi)^4 \delta^4(p_a + p_b - p_1 - p_2 - q) |\mathcal{M}_\gamma|^2 \frac{f_a(E_a)f_b(E_b)[1 + f_1(E_1)][1 + f_2(E_2)]}{2(2\pi)^3}, \quad (\text{A1})$$

we perform the integrations over the energy-momentum conserving delta function to obtain

$$\begin{aligned} q_0 \frac{dR^\gamma}{d^3q} &= \frac{N}{16(2\pi)^{11}} \int \frac{d^3p_a}{E_a} \frac{d^3p_b}{E_b} \int \frac{d^3p_1}{E_1} f_a f_b [1 + f_1][1 + f_2] \\ &\quad \times |\mathcal{M}_\gamma|^2 \delta((E_a + E_b - E_1 - q_0)^2 - (\mathbf{p}_a + \mathbf{p}_b - \mathbf{p}_1 - \mathbf{q})^2 - m_2^2) \\ &= \frac{N}{16(2\pi)^{11}} \int |\mathbf{p}_a| dE_a d\Omega_a \int |\mathbf{p}_b| dE_b d\Omega_b \int |\mathbf{p}_1| dE_1 d\Omega_1 f_a f_b [1 + f_1][1 + f_2] \\ &\quad \times |\mathcal{M}_\gamma|^2 \delta((E_a + E_b - E_1 - q_0)^2 - (\mathbf{p}_a + \mathbf{p}_b - \mathbf{p}_1 - \mathbf{q})^2 - m_2^2). \end{aligned} \quad (\text{A2})$$

We evaluate this equation by the Monte Carlo method, choosing the coordinates for each particle as follows,

$$\begin{aligned} p_a &= (E_a, |\mathbf{p}_a| \sin\theta_a \cos\phi_a, |\mathbf{p}_a| \sin\theta_a \sin\phi_a, |\mathbf{p}_a| \cos\theta_a), \\ p_b &= (E_b, |\mathbf{p}_b| \sin\theta_b \cos\phi_b, |\mathbf{p}_b| \sin\theta_b \sin\phi_b, |\mathbf{p}_b| \cos\theta_b), \\ p_1 &= (E_1, |\mathbf{p}_1| \sin\theta_1 \cos\phi_1, |\mathbf{p}_1| \sin\theta_1 \sin\phi_1, |\mathbf{p}_1| \cos\theta_1), \\ q &= (q_0, 0, 0, |\mathbf{q}|), \\ p_2 &= p_a + p_b - p_1 - q, \end{aligned} \quad (\text{A3})$$

with

$$E_i = \sqrt{m_i^2 + \mathbf{p}_i^2} \quad (i = a, b, 1, 2, q). \quad (\text{A4})$$

Thus, Eq. (A2) can be rewritten as

$$\begin{aligned} q_0 \frac{dR^\gamma}{d^3q} &= \frac{N}{16(2\pi)^{11}} \int |\mathbf{p}_a| dE_a \sin\theta_a d\theta_a d\phi_a \int |\mathbf{p}_b| dE_b \sin\theta_b d\theta_b d\phi_b \int |\mathbf{p}_1| dE_1 \sin\theta_1 d\theta_1 d\phi_1 f_a f_b [1 + f_1][1 + f_2] \\ &\quad \times |\mathcal{M}_\gamma|^2 \delta((E_a + E_b - E_1 - q_0)^2 - (\mathbf{p}_a + \mathbf{p}_b - \mathbf{p}_1 - \mathbf{q})^2 - m_2^2). \end{aligned} \quad (\text{A5})$$

In the argument of the delta function, one has

$$\begin{aligned} (\mathbf{p}_a + \mathbf{p}_b - \mathbf{p}_1 - \mathbf{q})^2 &= |\mathbf{p}_a|^2 + 2\mathbf{p}_a \cdot \mathbf{p}_b - 2\mathbf{p}_a \cdot \mathbf{p}_1 - 2\mathbf{p}_a \cdot \mathbf{q} + (\mathbf{p}_b - \mathbf{p}_1 - \mathbf{q})^2 \\ &= 2|\mathbf{p}_a||\mathbf{p}_b| \sin\theta_a \sin\theta_b \cos\phi_a \cos\phi_b + 2|\mathbf{p}_a||\mathbf{p}_b| \sin\theta_a \sin\theta_b \sin\phi_a \sin\phi_b + 2|\mathbf{p}_a||\mathbf{p}_b| \cos\theta_a \cos\theta_b \\ &\quad - 2|\mathbf{p}_a||\mathbf{p}_1| \sin\theta_a \sin\theta_1 \cos\phi_a \cos\phi_1 - 2|\mathbf{p}_a||\mathbf{p}_1| \sin\theta_a \sin\theta_1 \sin\phi_a \sin\phi_1 - 2|\mathbf{p}_a||\mathbf{p}_1| \cos\theta_a \cos\theta_1 \\ &\quad - 2|\mathbf{p}_a||\mathbf{q}| \cos\theta_a + |\mathbf{p}_a|^2 + (\mathbf{p}_b - \mathbf{p}_1 - \mathbf{q})^2. \end{aligned} \quad (\text{A6})$$

Upon integrating over  $\theta_a$ , we arrive at

$$q_0 \frac{dR^\gamma}{d^3q} = \frac{N}{16(2\pi)^{11}} \int |\mathbf{p}_a| dE_a d\phi_a \int |\mathbf{p}_b| dE_b \sin\theta_b d\theta_b d\phi_b \int |\mathbf{p}_1| dE_1 \sin\theta_1 d\theta_1 d\phi_1 f_a f_b [1 + f_1][1 + f_2] \frac{|\mathcal{M}_\gamma|^2}{\mathcal{A}} \quad (\text{A7})$$

with

$$\mathcal{A} = |\varphi'(\cos\theta_a^r)|. \quad (\text{A8})$$

In the above,  $\cos\theta_a^r$  is the root of function  $\varphi(\cos\theta_a)$ ,

$$\begin{aligned} \varphi(\cos\theta_a) &= (2|\mathbf{p}_a||\mathbf{p}_b| \sin\theta_b \cos\phi_a \cos\phi_b + 2|\mathbf{p}_a||\mathbf{p}_b| \sin\theta_b \sin\phi_a \sin\phi_b - 2|\mathbf{p}_a||\mathbf{p}_1| \sin\theta_1 \cos\phi_a \cos\phi_1 \\ &\quad - 2|\mathbf{p}_a||\mathbf{p}_1| \sin\theta_1 \sin\phi_a \sin\phi_1) \sqrt{1 - \cos^2\theta_a} \\ &\quad + (2|\mathbf{p}_a||\mathbf{p}_b| \cos\theta_b - 2|\mathbf{p}_a||\mathbf{p}_1| \cos\theta_1 - 2|\mathbf{p}_a||\mathbf{q}|) \cos\theta_a \\ &\quad + |\mathbf{p}_a|^2 + (\mathbf{p}_b - \mathbf{p}_1 - \mathbf{q})^2 - (E_a + E_b - E_1 - q_0)^2 + m_2^2 = 0. \end{aligned} \quad (\text{A9})$$

with

$$\begin{aligned} (\mathbf{p}_b - \mathbf{p}_1 - \mathbf{q})^2 &= |\mathbf{p}_b|^2 + |\mathbf{p}_1|^2 + |\mathbf{q}|^2 - 2|\mathbf{p}_b||\mathbf{p}_1|\sin\theta_b\sin\theta_1\cos\phi_b\cos\phi_1 - 2|\mathbf{p}_b||\mathbf{p}_1|\sin\theta_b\sin\theta_1\sin\phi_b\sin\phi_1 \\ &\quad - 2|\mathbf{p}_b||\mathbf{p}_1|\cos\theta_b\cos\theta_1 - 2|\mathbf{p}_b||\mathbf{q}|\cos\theta_b + |\mathbf{p}_1||\mathbf{q}|\cos\theta_1. \end{aligned} \quad (\text{A10})$$

There are two additional constraints on the eight integration variables in Eq. (A7):

- a. For any configuration of the eight variables, Eq. (A9) must have at least one root.
- b.  $E_a + E_b \geq E_1 + q_0 + m_2$ .

## APPENDIX B: GAUGE INVARIANCE OF PHOTON PRODUCTION AMPLITUDES

In this appendix, we demonstrate gauge invariance for the process  $\pi^+\pi^- \rightarrow \pi^+\pi^-\gamma$ . In this case the charges are,  $Q_a = Q_1 = 1$ ,  $Q_b = Q_2 = -1$ , and there is no  $u$ -channel contribution. To verify  $\mathcal{M}^\mu \cdot q_\mu = 0$  for the  $t$ -channel amplitude, we have

$$\begin{aligned} \mathcal{M}_t^\mu \cdot q_\mu &= e(J_a^\mu \mathcal{M}_t(p_a - q, p_b, p_1, p_2) + J_b^\mu \mathcal{M}_t(p_a, p_b - q, p_1, p_2) \\ &\quad + J_1^\mu \mathcal{M}_t(p_a, p_b, p_1 + q, p_2) + J_2^\mu \mathcal{M}_t(p_a, p_b, p_1, p_2 + q)) \cdot q_\mu \\ &= e(-\mathcal{M}_t(p_a - q, p_b, p_1, p_2) + \mathcal{M}_t(p_a, p_b - p_a, p_1, p_2) + \mathcal{M}_t(p_a, p_b, p_1 + q, p_2) - \mathcal{M}_t(p_a, p_b, p_1, p_2 + q) \\ &= eg_{\sigma\pi\pi}^2 \left\{ F^2[(p_b - p_2)^2] \left[ \frac{(p_a \cdot p_1 - q \cdot p_1)p_b \cdot p_2}{(p_b - p_2)^2 - m_\sigma^2 + im_\sigma\Gamma_\sigma} - \frac{(p_a \cdot p_1 + p_a \cdot q)p_b \cdot p_2}{(p_b - p_2)^2 - m_\sigma^2 + im_\sigma\Gamma_\sigma} \right] \right. \\ &\quad \left. + F[(p_a - p_1)^2] \left[ -\frac{p_a \cdot p_1(p_b \cdot p_2 - q \cdot p_2)}{(p_a - p_1)^2 - m_\sigma^2 + im_\sigma\Gamma_\sigma} + \frac{p_a \cdot p_1(p_b \cdot p_2 + p_b \cdot q)}{(p_a - p_1)^2 - m_\sigma^2 + im_\sigma\Gamma_\sigma} \right] \right\} \\ &= eg_{\sigma\pi\pi}^2 \left[ F^2[(p_b - p_2)^2] \frac{-(q \cdot p_1 + q \cdot p_a)p_b \cdot p_2}{(p_b - p_2)^2 - m_\sigma^2 + im_\sigma\Gamma_\sigma} + F^2[(p_a - p_1)^2] \frac{p_a \cdot p_1(q \cdot p_2 + q \cdot p_b)}{(p_a - p_1)^2 - m_\sigma^2 + im_\sigma\Gamma_\sigma} \right], \end{aligned} \quad (\text{B1})$$

so that the pertinent contact term is deduced as

$$\mathcal{M}_t^{(c)\mu} \cdot q_\mu = F^2[(p_b - p_2)^2] \frac{eg_{\sigma\pi\pi}^2(p_a \cdot q + p_1 \cdot q)p_b \cdot p_2}{(p_b - p_2)^2 - m_\sigma^2 + im_\sigma\Gamma_\sigma} - F^2[(p_a - p_1)^2] \frac{eg_{\sigma\pi\pi}^2 p_a \cdot p_1(p_b \cdot q + p_2 \cdot q)}{(p_a - p_1)^2 - m_\sigma^2 + im_\sigma\Gamma_\sigma}, \quad (\text{B2})$$

resulting in  $\mathcal{M}_t^\mu \cdot q_\mu + \mathcal{M}_t^{(c)\mu} \cdot q_\mu = 0$ . Similarly, for the  $s$ -channel, we have

$$\begin{aligned} \mathcal{M}_s^\mu \cdot q_\mu &= e(J_a^\mu \mathcal{M}_s(p_a - q, p_b, p_1, p_2) + J_b^\mu \mathcal{M}_s(p_a, p_b - q, p_1, p_2) \\ &\quad + J_1^\mu \mathcal{M}_s(p_a, p_b, p_1 + q, p_2) + J_2^\mu \mathcal{M}_s(p_a, p_b, p_1, p_2 + q)) \cdot q_\mu \\ &= e(-\mathcal{M}_s(p_a - q, p_b, p_1, p_2) + \mathcal{M}_s(p_a, p_b - p_a, p_1, p_2) + \mathcal{M}_s(p_a, p_b, p_1 + q, p_2) - \mathcal{M}_s(p_a, p_b, p_1, p_2 + q) \\ &= eg_{\sigma\pi\pi}^2 \left[ \frac{(p_a \cdot p_b - q \cdot p_b)p_1 \cdot p_2}{(p_1 + p_2)^2 - m_\sigma^2 + im_\sigma\Gamma_\sigma} - \frac{(p_a \cdot p_b - p_a \cdot q)p_1 \cdot p_2}{(p_1 + p_2)^2 - m_\sigma^2 + im_\sigma\Gamma_\sigma} \right. \\ &\quad \left. - \frac{p_a \cdot p_b(p_1 \cdot p_2 + q \cdot p_2)}{(p_a + p_b)^2 - m_\sigma^2 + im_\sigma\Gamma_\sigma} + \frac{p_a \cdot p_b(p_1 \cdot p_2 + p_1 \cdot q)}{(p_a + p_b)^2 - m_\sigma^2 + im_\sigma\Gamma_\sigma} \right] \\ &= eg_{\sigma\pi\pi}^2 \left[ \frac{-(q \cdot p_b - q \cdot p_a)p_1 \cdot p_2}{(p_1 + p_2)^2 - m_\sigma^2 + im_\sigma\Gamma_\sigma} + \frac{p_a \cdot p_b(q \cdot p_1 - q \cdot p_2)}{(p_a + p_b)^2 - m_\sigma^2 + im_\sigma\Gamma_\sigma} \right] \end{aligned} \quad (\text{B3})$$

and the required contact term follows as

$$\mathcal{M}_s^{(c)\mu} \cdot q_\mu = \frac{eg_{\sigma\pi\pi}^2(p_b \cdot q - p_a \cdot q)p_1 \cdot p_2}{(p_1 + p_2)^2 - m_\sigma^2 + im_\sigma\Gamma_\sigma} - \frac{eg_{\sigma\pi\pi}^2 p_a \cdot p_b(p_1 \cdot q - p_2 \cdot q)}{(p_a + p_b)^2 - m_\sigma^2 + im_\sigma\Gamma_\sigma}. \quad (\text{B4})$$

Again, we arrive at  $\mathcal{M}_s^\mu \cdot q_\mu + \mathcal{M}_s^{(c)\mu} \cdot q_\mu = 0$ . It is straightforward to test the rho-meson exchange channels along similar lines.

### APPENDIX C: RATE PARAMETRIZATION

The thermal production rate of photons from Bremsstrahlung off  $\pi\pi$  and  $\pi K$  scattering as employed in Sec. VI can be conveniently parametrized as

$$\begin{aligned}
 q_0 \frac{dR_{\pi\pi}}{d^3q} &= \frac{-0.00026421 + \frac{0.0075394}{0.13007\sqrt{\pi/2}} \exp\left[\frac{-2(T-0.28351)^2}{0.13007^2}\right]}{0.01277} \\
 &\quad \times \frac{-0.00018184 + \frac{0.00073983}{\pi[4(q_0-0.054587)^2+0.099656^2]}}{[1.+104(0.18-T)^{1.4}(q_0-0.1)]}, \\
 q_0 \frac{dR_{\pi K}}{d^3q} &= \frac{-0.0000411907 + \frac{0.0013114}{0.12037\sqrt{\pi/2}} \exp\left[\frac{-2(T-0.27292)^2}{0.12037^2}\right]}{0.00227} \\
 &\quad \times \frac{-0.000021454 + \frac{0.0001459}{\pi[4(q_0-0.043159)^2+0.085668^2]}}{[1.+605(0.18-T)^{1.7}(q_0-0.1)]}
 \end{aligned} \tag{C1}$$

These expressions reproduce the exact rates within  $\sim 3\%$  in the energy interval between 0.1 GeV and 0.5 GeV and in the temperature range 0.1-0.18 GeV. Pion and kaon chemical potentials are included as  $\mu_\pi(T)$  and  $\mu_K(T)$  according to the fireball evolution employed in this work for central  $Pb(158 \text{ AGeV})-Pb$  collisions, cf. eq. (16).

---

[1] J. Alam, S. Sarkar, P. Roy, T. Hatsuda and B. Sinha, *Annals Phys.* **286**, 159 (2001).  
[2] T. Peitzmann and M.H. Thoma, *Phys. Rep.* **364**, 175 (2002).  
[3] R. Rapp, *Mod. Phys. Lett.* **A19**, 1717 (2004).  
[4] J. Kapusta, P. Lichard, and D. Seibert, *Phys. Rev. D* **44**, 2774 (1991).  
[5] C. Song, *Phys. Rev. C* **47**, 2861 (1993).  
[6] V.V. Goloviznin and K. Redlich, *Phys. Lett.* **B319**, 520 (1993).  
[7] P.K. Roy, D. Pal, S. Sarkar, D.K. Srivastava and B. Sinha, *Phys. Rev. C* **53**, 2364 (1996).  
[8] J. Alam, P. Roy, and S. Sarkar, *Phys. Rev. C* **68**, 031901 (2003).  
[9] S. Turbide, R. Rapp, and C. Gale, *Phys. Rev. C* **69**, 014903 (2004).  
[10] D.K. Srivastava, *Phys. Rev. C* **71**, 034905 (2005).  
[11] WA98 Collaboration (M. M. Aggarwal *et al.*), *Phys. Rev. Lett.* **85**, 3595 (2000).  
[12] WA98 Collaboration (M. M. Aggarwal *et al.*), *Phys. Rev. Lett.* **93**, 022301 (2004).  
[13] S. Turbide, private communication (2004).  
[14] R. Rapp, arXiv:nucl-th/0502020.  
[15] R. Rückl, *Phys. Lett.* **B64**, 39 (1976).  
[16] H.C. Eggers, R. Tabti, C. Gale, and K. Haglin, *Phys. Rev. D* **53**, 4822 (1996).  
[17] J. Cleymans, V. V. Goloviznin, and K. Redlich, *Phys. Rev. D* **47**, 173 (1993).  
[18] J. Knoll and R. Lenk, *Nucl. Phys.* **A561**, 501 (1993).  
[19] C.H. Li and C.M. Ko, *Nucl. Phys. A* **712**, 110 (2002).  
[20] J. F. Donoghue, C. Ramirez, and G. Valencia, *Phys. Rev. D* **39**, 1947 (1989).  
[21] K. Haglin, C. Gale, and V. Emelyanov, *Phys. Rev. D* **47**, 973 (1993).  
[22] V. Srinivasan *et al.*, *Phys. Rev. D* **12**, 681 (1975); S. D. Protopoescu *et al.* *Phys. Rev. D* **7**, 1279 (1973).  
[23] A. Firestone, G. Goldhaber, D. Lissauer, and G. H. Trilling, *Phys. Rev. D* **5**, 2188 (1972).  
[24] R. Rapp, *Phys. Rev. C* **66**, 017901 (2002).  
[25] R. Rapp and J. Wambach, *Eur. Phys. J. A* **6**, 415 (1999).  
[26] L. Landau and I. Pomeranchuk, *Dokl. Akad. Nauk SSSR* **92**, 535 (1953); **92**, 735 (1953); A. B. Migdal, *Dokl. Akad. Nauk SSSR* **96**, 49 (1954); *Phys. Rev.* **103**, 1811 (1956).  
[27] R. Rapp and J. Wambach, *Phys. Lett.* **B315**, 220 (1993).  
[28] R. Rapp and J. Wambach, *Nucl. Phys.* **A573**, 626 (1994).  
[29] G. Agakichiev *et al.* [CERES Collaboration], *Eur. Phys. J. C* **41**, 475 (2005).  
[30] S. Damjanovic *et al.* [NA60 Collaboration], arXiv:nucl-ex/0510044.  
[31] H. van Hees and R. Rapp, arXiv:hep-ph/0603084.  
[32] N. Grion *et al.* [CHAOS Collaboration], *Nucl. Phys.* **A763**, 80 (2005).  
[33] A. Starostin *et al.* [Crystal Ball Collaboration], *Phys. Rev. Lett.* **85**, 5539 (2000).  
[34] T. Hatsuda, T. Kunihiro, and H. Shimizu, *Phys. Rev. Lett.* **82**, 2840 (1999).  
[35] D. Cabrera, E. Oset and M.J. Vicente Vacas, *Phys. Rev. C* **72**, 025207 (2005).  
[36] D. Röder, arXiv:hep-ph/0509232.  
[37] M.A. Halasz, J.V. Steele, G.Q. Li and G.E. Brown, *Phys. Rev. C* **58**, 365 (1998).

- [38] C.s. Song and G. I. Fai, Phys. Rev. C **58**, 1689 (1998).
- [39] J.e. Alam, P. Roy, S. Sarkar and B. Sinha, Phys. Rev. C **67**, 054901 (2003).
- [40] P. Arnold, G.D. Moore and L.G. Yaffe, JHEP 0112 (2001) 009.
- [41] R. Rapp, M. Urban, M. Buballa and J. Wambach, Phys. Lett. **B417**, 1 (1998).
- [42] J. Bjorken and L. McLerran, Phys. Rev. D **31**, 63 (1985).
- [43] C.M. Ko and C.Y. Wong, Phys. Rev. C **33**, 153 (1986).
- [44] NA49 Collaboration (J. Bächler *et al.*), Nucl. Phys. **A661**, 45c (1999).
- [45] The relevance of the final-state enhancement factors in hadronic phase of URHICs is further augmented by the build-up of substantial pion- and kaon-chemical potentials after chemical freezeout [24].